Determining the Jet Opening Angle of Cosmic Gamma-Ray Bursts

by

Erica L. McEvoy

Submitted to the Department of Earth, Atmospheric, and Planetary Sciences
in partial fulfillment of the requirements for the degree of

Master of Science in Planetary Science

at the

MASSACHUSETTS INSTITUTE OF TECHNOLOGY
[September 2005]
August 2005

Author .....
Department of Earth, Atmospheric, and Planetary Sciences
August 31, 2005

Certified by .....
Paul C. Joss
Professor
Thesis Supervisor

Accepted by .....
Maria Zuber
Chairman, Department Thesis Coordinator

Determining the Jet Opening Angle of Cosmic Gamma-Ray Bursts

by

Erica L. McEvoy

Submitted to the Department of Earth, Atmospheric, and Planetary Sciences
on August 31, 2005, in partial fulfillment of the
requirements for the degree of
Master of Science in Planetary Science

Abstract

There is growing scientific agreement that at least some cosmic gamma-ray bursts (GRBs) coincide with the deaths of rapidly rotating massive stars – dubbed "hypernovae." In 1987, a supernova (SN 1987A) was detected in the Large Magellanic Cloud – its progenitor was a blue, rapidly rotating supergiant that was a likely member of a binary system that underwent merger prior to the supernova event [1]. Although no accompanying GRB was detected, there is evidence [2] that one may have occurred but was beamed in a direction away from the Earth. Whether or not SN 1987A was a hypernova or generated a GRB, we can investigate the question: Are long duration GRBs produced by hypernovae, and are massive interacting binary systems the progenitors of hypernovae?

In this thesis, we use a phenomenological model to determine θ, the jet opening angle of long duration GRBs. Our basic underlying assumption is that massive binary star sytems are hypernova progenitors. We also test the hypothesis that these systems do not undergo significant cosmological evolution. We find that the statistics of GRBs are, in fact, consistent with a uniform rate per unit of comoving volume from $z \simeq 3$ to the present, and we incorporate this result in our model. We calculate θ by deriving two expressions for the probability that a given GRB is detected, one based on the geometry implied by the beaming model and the other based on the observed and expected rates of long duration GRBs, under the assumption that these events are produced by hypernovae that originate in massive, interacting, binary systems. These expressions give the detection probability as a function of a few key physical parameters. By finding estimates of these parameters, equating the two expressions, and performing a Monte Carlo simulation, we obtain the most probable value of θ for single-jet and double-jet burst models.

For the single-jet burst model, we find that the most probable value is 8^{+6}_{-3} deg (FWHM), the median value is 10.3 deg, and the standard deviation is 4.4 deg. For the double-jet model, we find that the most probable and median values are $5.5^{+3}_{-1.5}$

deg, and 7.3 deg, respectively, and a standard deviation of 3.1 deg.

Because these results are well in agreement with values inferred from the observed properties of long duration GRBs [3] and with values calculated based on the structured jet model of these bursts [4], we conclude that our underlying assumption – that massive, binary systems are hypernovae progenitors – is at the very least plausible and is consistent with the hypothesis that SN 1987A was a prototypical hypernova event. Futhermore, our result from applying a statistical test to the distribution of long duration GRBs in space allows us to conclude that these events (and their progenitors) are likely to have a uniform density in comoving space out to cosmological distances ($z \simeq 3$).

Thesis Supervisor: Paul C. Joss
Title: Professor

Acknowledgments

This paper is dedicated to my family and the friends I've acquired during my time at MIT – their love, support, and camaraderie have opened many doors for me and made everything possible.

I would like to thank my advisor, Paul Joss, for his guidance, support, insight, and boundless enthusiasm throughout our time working together. I have learned a great deal from our meetings, and am looking forward to future projects together.

I would also like to thank Prof. Jack Wisdom for his encouragement and support this past year, and Yelena Tsitkin for saving me countless hours with figures and assistance with the bibliography.

A very special thank you goes to Nick Fotopoulos for his generous help in editing, assistance with Matlab and LaTeX, providing clarifications and corrections during many parts of this project, humor, and endless patience and support. Much of this thesis would not have been completed without him.

Finally, I would like to thank Dhanesh Samarasan for his invaluable help and guidance during the beginning stages of this work. His enduring support is what made the beginnings of this project possible in the first place.

Contents

List of Figures

List of Tables

Chapter 1

Introduction

The energetics of gamma-ray bursts (GRBs) are extreme - assuming isotropic emission, one can calculate as much as $2M_{\odot}c^2$ worth of energy in a single burst. It is difficult to conceive of physical models which could produce such high emission energies on such short timescales. A popular model for GRBs is that of a hypernova, which is a massive, rapidly rotating core collapse supernova. Hypernovae are thought to form beamed jets of γ-radiation; the beaming reduces the energetics to tractable proportions. In this thesis, we assume that long-duration GRBs and hypernovae are one and the same, and use this assumption to calculate θ, the jet opening angle of GRBs.

Knowledge of θ is a valuable litmus test of GRB progenitor models, which can strengthen or weaken the plausibility of this model. For many approaches, θ is an accessible quantity, both theoretically and observationally, and is therefore useful in constraining possible progenitor models. For example, knowlege of θ tells us about the proper energy emission geometry and jet structure (energy distribution) [5], which is required to find the total energy release within the burst (a requirement for hypernova physics to satisfy). Since the hypernova scenario has only a limited range of allowable opening angles, knowledge of the opening angle sheds light into the physics behind the hypernova event itself.

In addition to calculating θ, we will also adopt a statistic that allows us to test the uniformity of GRBs over cosmological distances.

Supernova 1987A (SN 1987A hereafter) was the closest naked-eye supernova in over 300 years, occuring in the Large Magellanic Cloud (LMC). Its progenitor, star Sk $-69^{\circ}202$, was a blue supergiant that resembled a typical, unevolved star in the LMC, was most unusual for a supernova progenitor. Furthermore, the discovery of neutrinos from the supernova explosion, along with the energies and spread in arrival times of these neutrinos, provided compelling evidence that core collapse had occured. However, in many ways, SN 1987A did not comply with standard theoretical expectations. It was exactly this noncompliance that prompted theorists to consider binary involvement of the progenitor star as an alternative [1, 6].

Further theroetical work has demonstrated that the progenitor of SN 1987A was likely to have been the end-product of a stellar merger in a massive binary system. Along with other evidence, this suggests that SN 1987A might have been a hypernova and may even have generated a GRB event for observers within the beams of the hypernova jets.

In the next section, we will paint the history of GRB observation and theory. Further details regarding GRB detection and observations are provided in §1.2 and §1.3.

1.1 Detecting Gamma-Ray Bursts and Hypernovae

In the 1960s, the U.S. Air Force launched a series of satellites inspired by a recently signed nuclear test ban treaty. These satellites — named "Vela" — were part of a classified research and development program whose goal was to develop the technology to monitor nuclear tests from space and give the U.S. a means of verifying

compliance with the conditions of the treaty. At the end of the decade, while examining archived data from the Vela 4 satellite, Ray Klebesadel and Roy Olsen, both of the Los Alamos National Laboratory, discovered a mysterious event that had been recorded a few years earlier. It appeared to be a short burst of gamma rays, lasting approximately 6 seconds. At the time, the technology was insufficient to determine where the burst occurred. As a result, because of Cold War suspicions about its possible terrestrial origin, the Vela findings remained classified until 1973, by which time it had become clear that this burst, and other similar events discovered by Vela, were of cosmic origin [7].

In 1976, the Interplanetary Network (IPN) was launched. It comprised a set of gamma-ray detectors aboard solar and planetary spacecraft, used to locate the position of a GRB using triangulation. By locating these bursts to within a few arc minutes, the IPN was able to show that GRBs were not already known sources of interest (such as X-ray emitters).

In 1991, NASA launched the Burst and Transient Source Experiment (BATSE) aboard the Compton Gamma-Ray Observatory. Its primary goal was to study the (poorly understood) phenomenon of GRBs by detecting and recording them as they happened. Similar projects with more advanced capabilities were later launched: the Italian-Dutch BeppoSAX satellite, the High-Energy Transient Explorer II (HETE-2), INTEGRAL, and Swift.

By 1992, it had become clear that GRBs are bimodal: 75 % are "long," with mean durations of $\simeq$ 20 s; while the remainder are much shorter, with a mean of only $\simeq$ 0.2 s [8, 9]. Given the clear distinction between the two types, it appeared that there were two separate causes at work, i.e., two types of progenitors. In this thesis, we focus on the physics of long-duration GRBs only; unless otherwise stated, we shall use the term GRBs in Chapters 2 and 3 only for long-duration bursts.

By 1995, over 500 GRBs had been detected by BATSE and their angular positions in the sky recorded – but the distances to the sources remained unknown. A plot of all detected GRB sites showed that they were randomly distributed across the entire sky, with no significant concentration towards the galactic center or plane (Figure 1-1), thus suggesting that they were at cosmological distances, rather than of galactic origin. If this were the case, then GRBs – detected as powerful sources notwithstanding their cosmological distances – posed a problem: how to explain what would be the most luminous and energetic sources of electromagnetic radiation known in the universe (releasing $\simeq 10^{51}$-10^{54} ergs per burst in γ-rays alone!).

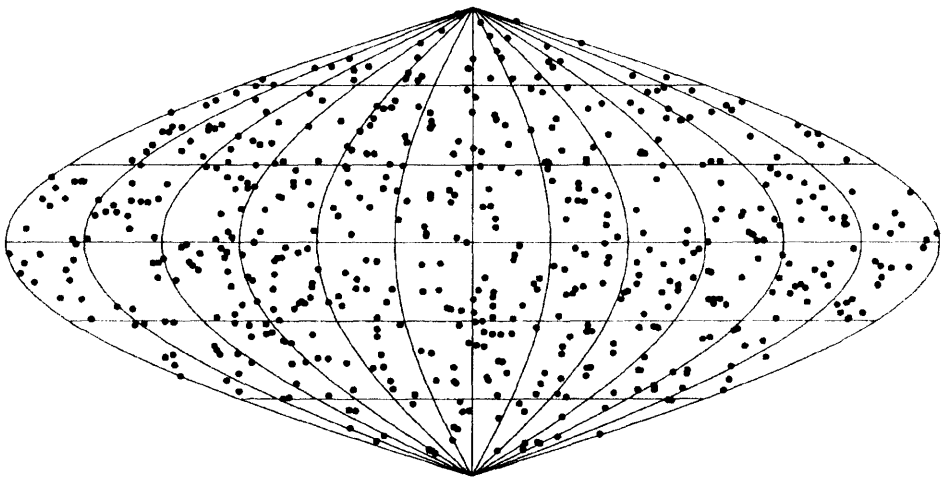

Figure 1-1: *The distribution of 535 GRBs detected as of 1995 from the second BATSE catalog [10]. The apparent isotropy suggests that GRBs are of cosmological, rather than galactic, origin.*

An early attempt to explain these large bursts of energy was based on the merger of neutron stars. It was known that binary neutron stars (NS-NS) sometimes merge because of the emission of gravitational radiation from their binary orbits. These mergers might radiate large amounts of energy in the form of gamma-rays, and thus could account for both the observed energetics and the random distribution of GRBs [11, 12]. So were NS-NS mergers really the source of GRBs?

When an NS-NS system is formed, the two formative supernova explosions in the progenitor binaries propel the stars at high recoil velocities (a natal "kick") so that, given the very long merger timescale, the merging neutron stars have the potential to travel far from their host galaxies [13]. If a GRB occurs when the neutron stars merge outside their home galaxies, then there should be no optical trace of their galaxies of origin.

In 1997, the discovery of an optical counterpart ("afterglow") to GRB 970228 made it possible for the first time to identify a host galaxy and thereby determine the redshift associated with a GRB. Calculations based on that and subsequent GRBs have by now confirmed that they do indeed occur at cosmological distances. Further analysis revealed that GRBs occur not outside their host galaxies (as the NS-NS theory would have it), but within the dense and dusty active star-forming regions of a host galaxy [14, 15, 16, 17, 18, 19, 20].

In 1998, an alternative explanation for the genesis of GRBs was suggested by Paczynski [16]. To solve the energy budget problem, he proposed that GRBs often accompany a hypernova explosion and the resulting creation of a "microquasar". A hypernova is thought to be a supernova event that results in the emission of γ radiation within narrow beams; the beaming of the emission greatly reduces the prodigious energy requirements. A microquasar is simply a "small" quasar (where the mass of the central black-hole is of the order of several $M_\odot$ instead of hundreds of $M_\odot$). According to the "collapsar model" of hypernovae [21, 16], the standard model which we will adopt, a GRB could be created in the following way: an initially massive, rapidly rotating star undergoes core collapse (the hypernova). This leads to the formation of a rapidly rotating (Kerr) black hole surrounded by a massive orbiting torus of debris. Energy is then extracted by the hole-torus interaction and is emitted as jets pointed along the axis of rotation, thereby forming a microquasar [16, 22, 23]. As Voss and Tauris [13] explain, hypernovae "are expected to be found close to their place of birth as a result of the short lifetime [...] of their progenitors". That is to say, if hyper-

novae produce these GRBs, one would expect to find such GRBs occurring in active star-forming regions (spiral arms) of galaxies, exactly where they are observed to be.

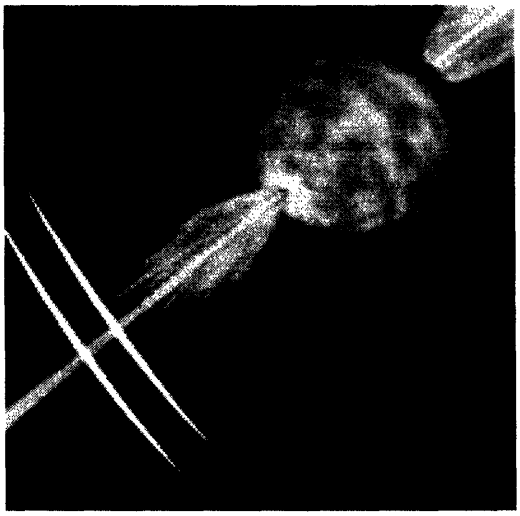

Figure 1-2: *An artist's rendition of a hypernova and its collimated jets. Here, the inner stellar core has collapsed and created the microquasar, whose jets are pictured puncturing the outer envelope of the progenitor star.*

More recent GRB observations have provided additional and stronger evidence of the link between hypernovae (i.e., some core collapse supernovae) and GRBs. For example, relatively nearby GRB 030329 ($z = 0.17$) had an unusually bright optical afterglow, making possible extensive observations of its optical spectrum. About a week after the GRB event, the observed spectrum changed suddenly to resemble that of SN1998bw, thus providing the first direct, spectroscopic confirmation that a subset of classical GRBs is caused by hypernovae [24].

1.2 Observational properties of GRBs

GRBs exhibit a wide variation of timescales. BATSE obervations of over 200 bursts illustrate that the timescales follow a bimodal distribution (Figure 1-3). Long-duration GRBs have durations from a few to hundreds of seconds, while short-duration GRBs

are typically tenths of seconds long, with the dividing line at $\simeq 2$ seconds. Furthermore, there exist differences in peak photon energies of bursts according to their durations (see Figure 1-3). It is thus thought that there are two different causes at work for the two different classes of bursts.

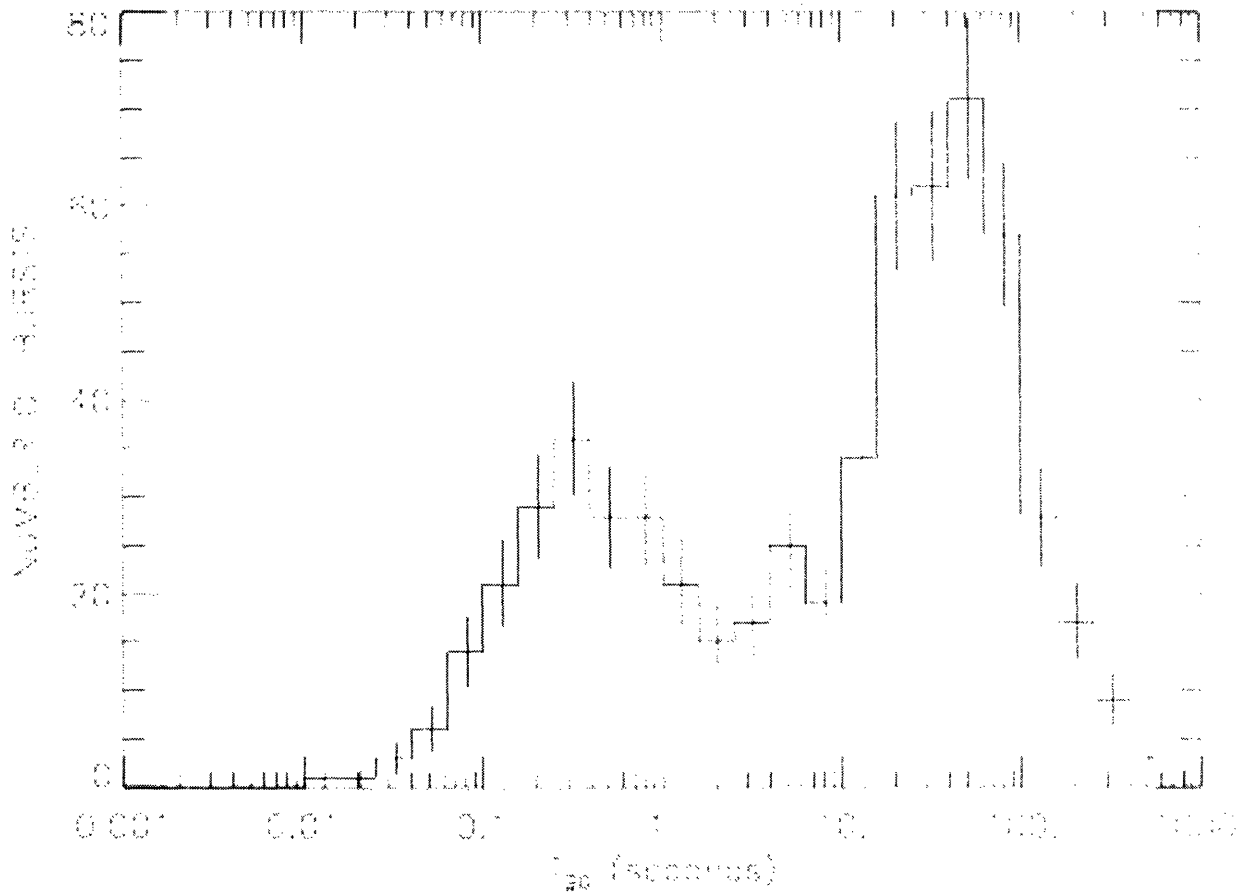

Figure 1-3: *Histogram of GRB durations for over 200 bursts detected by BATSE. Notice their bimodal distribution.*

In addition to their timescales, GRBs differ greatly in their light curves (Figure 1-4). Some may display a single, primary burst. Others may consist of a series of pulses of different heights and durations. Some pulses rise and/or fall very quickly, while others may rise or fall off more slowly.

Oftentimes a GRB is followed by transients and/or afterglows in other energy

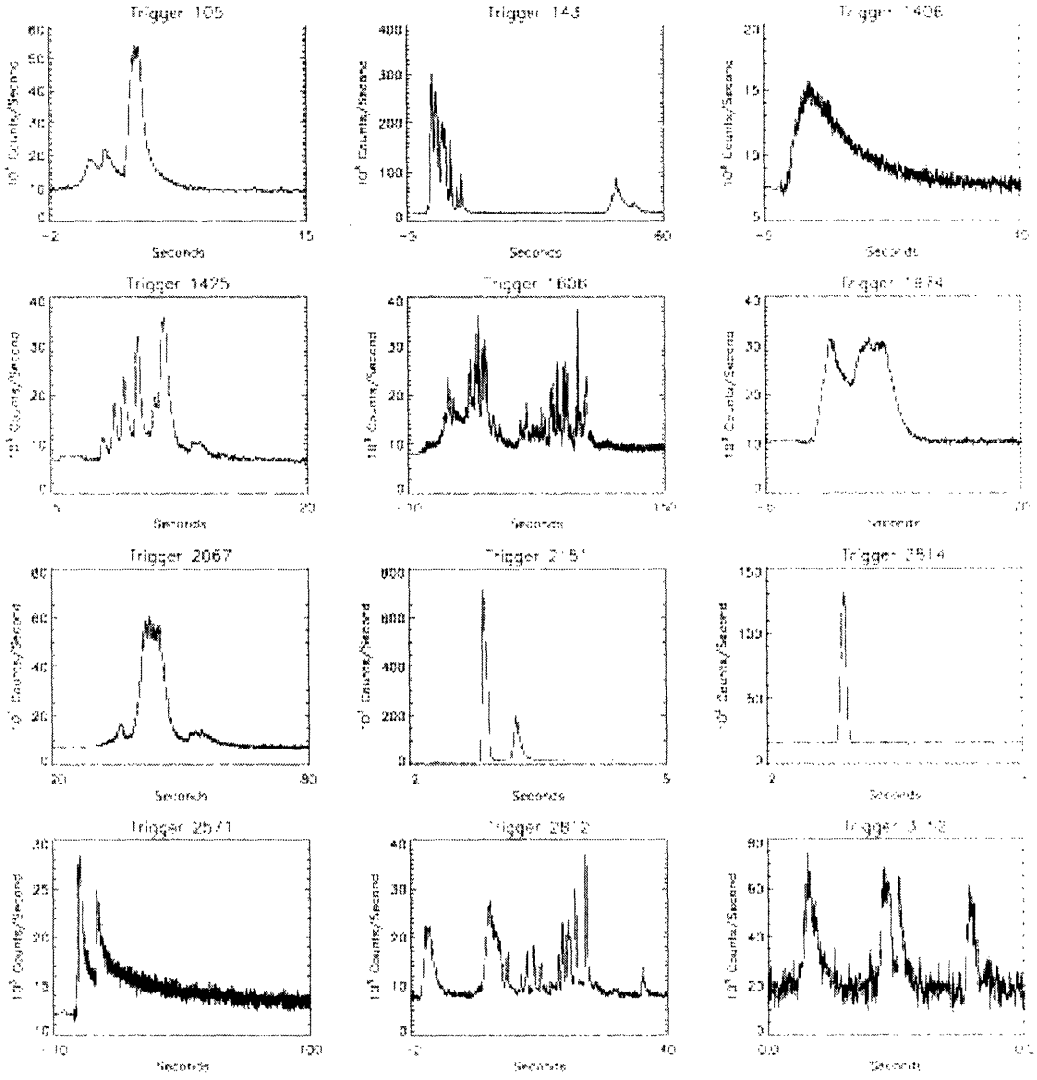

Figure 1-1: *GRB lightcurves come in an assorted variety of shapes, sizes, and number of pulses.*

bands (e.g., optical, X-ray, or radio). The optical afterglows have proven to be particularly useful in that they have allowed us to identify host galaxies, and subsequently determine their redshifts. Thus far, bursts have been observed as far as $z \approx 4$, with the majority clustered near $z \approx 1$. It is through these bursts with measured redshifts that we can determine θ.

1.3 Detection capabilities

In 1991, NASA launched the Burst and Transient Source Experiment (BATSE) aboard the Compton Gamma-Ray Observatory. Made up of four seperate detecting channels, it detected bursts with γ-ray energies between 50 and 300 keV. While good for its time, the instruments were only able to provide a burst position accurate to roughly 5 square degrees on the sky, thus leaving a relatively large positional error circle. Detecting over 2000 GRBs during its lifetime, BATSE provided the key information to deduce that GRBs are at cosmological distances. BATSE was decommisioned in August of 1996.

In 1996, the Gamma-Ray Burst Monitor (GRBM) was launched aboard the BeppoSAX space mission by the Italian Space Agency and the Netherlands Agency for Aerospace Programs. Its main mission was to provide a broader energy band for detecting GRBs, ranging from 40 to 700 keV. BeppoSAX also had a larger effective area for collecting GRB photons, as well as improved energy resolution and imaging capabilities compared to those of BATSE. It was the first instrument to provide burst positions accurate to a few arcminutes and to report positional determinations on a more rapid time scale. This made it possible to optically image a burst source soon after the burst event itself, thus making optical observations and redshift-measurements possible. BeppoSAX was decommissioned in April 2002.

In October of 2000, the (MIT constructed) High-Energy Transient Explorer II (HETE-2) was launched; the original HETE was lost during its launch. It included a set of wide-field gamma-ray spectrometers called FREGATE (French Gamma Telescope). The primary goal of HETE-2 was to determine the origin and nature of GRBs through studying their properties in X-ray and γ-ray energies from 6 to 400 keV), while providing precise localization and identification of burst sources. HETE-2 is still in operation today.

The European astronomical satellite, INTEGRAL, was launched in October of 2002. A medium-sized mission, INTEGRAL is planned to be in commission only for a few years. INTEGRAL was the first satellite to observe burst sources simultaneously in optical, X-ray, and γ-ray wavelengths, while having improved resolution and sensitivity.

The Burst Alert Telescope (BAT) is the gamma-ray instrument aboard the Swift mission, launched in November of 2004. As a NASA mission with international participation, Swift gives even more rapid timescales for burst localizations, allowing greater opportunity to observe the burst afterglow with ground and space-based telescopes. It also has instruments that work together to observe burst afterglows in γ-ray, X-ray, UV, and optical wavelengths, and provides redshifts for the bursts. To date, Swift provides the most comprehensive study of burst afterglows. However, data from this mission are not yet publicly released, and, therefore, will not be included in this thesis.

1.4 Synopsis of the thesis

In Chapter 2, we create a phenomenological model to predict the opening angle, θ, of a GRB jet by inferring the unknown frequency of hypernovae from the apparent frequency of this particular supernova type. We also compute estimates for a few key physical variables that arise in our equation for θ. In Chapter 3, we assemble our results and perform a Monte Carlo simulation to get a range of possible values for θ. We discuss and interpret these results. In particular, we re-examined the possibility that SN 1987A was a hypernova in light of our findings. At the end of Chapter 3, we discuss some areas for future research that might shed further light of the questions that we have addressed.

Chapter 2

A phenomenological model to determine jet opening angles of GRBs

In this thesis, we assume that GRBs derive from hypernovae, which we assume to be massive, rapidly rotating supernova events. With this as our starting point, we derive two expressions for the probability, P_{detect}, that a given GRB jet is detected and we estimate θ by equating these expressions.

Suppose a GRB with jet opening angle θ occurs at the center of a sphere of radius r. Then imagine there is an observer somewhere on the surface of that sphere (Figure 2.1). The probability of detecting a burst is the ratio of solid angle subtended by the GRB beam(s) to that of the entire sphere. For a GRB that emits a single jet:

$$P_{\text{detect, 1}} = \frac{2\pi r^2 \left(1 - \cos\left(\frac{\theta_1}{2}\right)\right)}{4\pi r^2} = \frac{1}{2}\left(1 - \cos\left(\frac{\theta_1}{2}\right)\right) \tag{2.1}$$

A GRB that emits a double jet (Figure 2.1) will subtend twice the solid angle on the spherical surface than that of a single jet:

$$P_{\text{detect, 2}} = \frac{4\pi r^2 \left(1 - \cos\left(\frac{\theta_2}{2}\right)\right)}{4\pi r^2} = 1 - \cos\left(\frac{\theta_2}{2}\right) \tag{2.2}$$

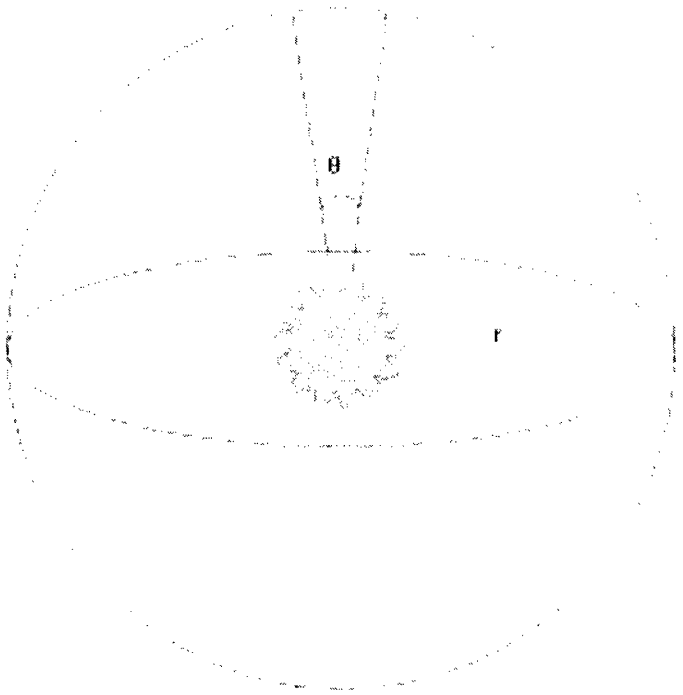

Figure 2-1: *Given a sphere with radius r, and a GRB centered inside the sphere, the probability of detection is given by the ratio of solid angles subtended by the beam(s) of the GRB to that of the entire sphere. Whether a GRB emits one or two beams of γ raditation is unknown. The dotted lines represent a (possible) second jet, in an opposing direction to the first beam.*

Notice that in both cases, P_{detect} is independent of r, i.e., independent of the distance from the observer. Also notice that if two beams were produced from the source, a point of contention, then an observer is twice as likely to be in the beamed region, and hence, P_{detect} for a two-jet burst is double that of a one-jet burst. Finally, notice that in the limit of small θ_1, $\theta_1 \simeq \sqrt{2}\theta_2$. Whether or not a GRB emits two jets of γ-radiation or just a single one is an open question. In this thesis, we will calculate θ for both single and double jet models.

Another way to calculate P_{detect} is, by definition, to find the fraction of all GRBs that are actually detected:

$$P_{detect} = \frac{R_{obs}}{R_{exp}} \tag{2.3}$$

Here, R_{obs} represents the rate of observed (detected) GRBs on Earth, and R_{exp} is the expected (or true) rate of GRBs that occur throughout space (detected or not). Because only the ratio of observed to expected bursts is needed, the units of "rate" are arbitrary.

Equating expressions 2.1 and 2.2 with 2.3, we can solve for θ:

$$\theta_1 = 2\cos^{-1}\left(1 - 2\frac{R_{obs}}{R_{exp}}\right) \tag{2.4}$$

$$\theta_2 = 2\cos^{-1}\left(1 - \frac{R_{obs}}{R_{exp}}\right) \tag{2.5}$$

In the following sections, we derive estimates for the quantities R_{obs} and R_{exp}, and use them to calculate values of θ.

2.1 Calculating R_{obs} - the observed rate of GRBs

In this section, we calculate the observed rate of GRBs. We choose the units of "rate" to be $\mathrm{Mpc}^{-3}\,\mathrm{yr}^{-1}$. We assume that this rate is separable, in the sense that it can be expressed in the form:

$$R_{obs} = \frac{\rho_{obs}}{\Delta T} \tag{2.6}$$

Here, ρ_{obs} is defined as the volume density of burst sources that have been detected, and ΔT is the total length of observation.

2.1.1 Calculating the observed volume density, ρ_{obs}

Consider a GRB that occurs somewhere in space. When a burst occurs and is detected, there are two factors that effect the probability of viewing that burst, assuming the burst jet points in our direction – the intrinsic brightness of the burst, and the

distance to the burst. Brighter bursts and closer bursts are more likely to be visible. Therefore, for a given brightness there must exist a maximum distance, or cosmological redshift, at which a burst can be detected. For such a redshift, there exists a corresponding maximum volume of detectability, V_{max}, that encloses the burst. This is the quantity we use to calculate volume densities. For a single burst, the volume density is $1/V_{max}$. For N bursts with measured redshift, the volume density is simply the sum over all bursts:

$$\rho_{obs} = \eta \sum_{i=1}^{N} \frac{1}{V_{max,i}} \tag{2.7}$$

where η is the ratio of the total number of detected bursts to the number of detected bursts with observationally measured redshifts. To calculate V_{max} from z_{max}, we use the following equation:

$$V_{max} = \frac{4}{3}\pi d_{max}^3 \tag{2.8}$$

where d_{max} represents the total line-of-sight comoving distance [25] corresponding to redshift, z_{max}, and is given by:

$$d_{max} = \frac{c}{H_0} \int_0^{z_{max}} \frac{dz}{\sqrt{\Omega_M (1+z)^3 + \Omega_k (1+z)^2 + \Omega_\Lambda}}. \tag{2.9}$$

Here, c is the speed of light, H_0 is the Hubble constant (which we take to be 70 $\mathrm{kms^{-1}Mpc^{-3}}$) [26], and Ω_M, Ω_k, and Ω_Λ are cosmological parameters that represent the partition of energy density throughout the universe. We adopt recent estimates for these parameters [26]: $\Omega_M = 0.3$, $\Omega_k = 0$, and $\Omega_\Lambda = 0.7$.

With the mathematical underpinnings in place, the first step in calculating V_{max} is to find an expression for z_{max} and calculate values for each burst. Qualitatively, this should depend on the measured "brightness" of the burst, the sensitivity of the detector(s), and the actual distance to the burst source, z_s. If a burst occured at its maximum possible redshift, z_{max}, then by definition, the incident photon flux would

register at the threshold of the detector. Therefore, if we know the threshold for GRB detection and the absolute luminosity (or time integrated luminosity) of the source (deduced from the measured redshift, z_s), we can find a z_{max} such that the perceived (measured) "signal" of the burst is equal to the detection threshold. Quantifying this concept requires understanding how GRB detectors work and finding their corresponding thresholds.

GRB detectors generate event triggers when they receive signal above some threshold. A signal is typically measured as a photon flux (photons cm^{-2} s^{-1}) or a fluence (photons cm^{-2} s^{-1} keV^{-1}). Bursts are typically triggered when the signal is some number of standard deviations above the background (noise) signal. In addition to the integrated energy flux (or fluence) of a burst, individual photon energies are recorded, and, by histogramming, one can obtain an energy spectrum (photons cm^{-2} s^{-1} keV^{-1} as a function of photon energy). Most GRB energy spectra share the same characteristic shape, and Band [27] has proposed the following approximation to fit them:

$$N(E) = \begin{cases} N_0 \left(\frac{E}{100\text{ keV}}\right)^{\alpha} e^{-\frac{E}{E_0}} & , E \leq E_b \\ N_0 \left(\frac{E_b}{100\text{ keV}}\right)^{\alpha-\beta} e^{\beta-\alpha} \left(\frac{E}{100\text{keV}}\right)^{\beta} & , E > E_b \end{cases} \tag{2.10}$$

In Band's expression, the fitted parameters are E_0, α (the low-energy spectral photon index), β (the high energy spectral photon index), E_b (the breaking energy of the burst, which is the value of E at which the power laws are joined), and the normalization constant, N_0 [1]. In some cases, bursts only display spectra visible in higher ($E > E_b$) or lower ($E < E_b$) energy ranges. In those cases, only the corresponding function for that energy range is used for fitting the spectrum.

To find z_{max}, we obtain the spectral parameters [28, 29, 30] for bursts with known

[1] From these parameters, another useful parameter can be derived, the peak energy, E_p. To find the maximum of $G(E) = E^2N(E)$, take the first derivative $\frac{dG}{dE}$, set equal to 0, and solve for E_p: $\frac{dG}{dE} = N_0(\alpha+2)\left(\frac{E_p}{100keV}\right)^{\alpha+2-1} e^{-\frac{E_p}{E_0}} + N_0(\frac{-1}{E_0})\left(\frac{E_p}{100keV}\right)^{\alpha+2} e^{-\frac{E_p}{E_0}} = 0$. Solving for E_p gives $E = (\alpha+2)E_0$.

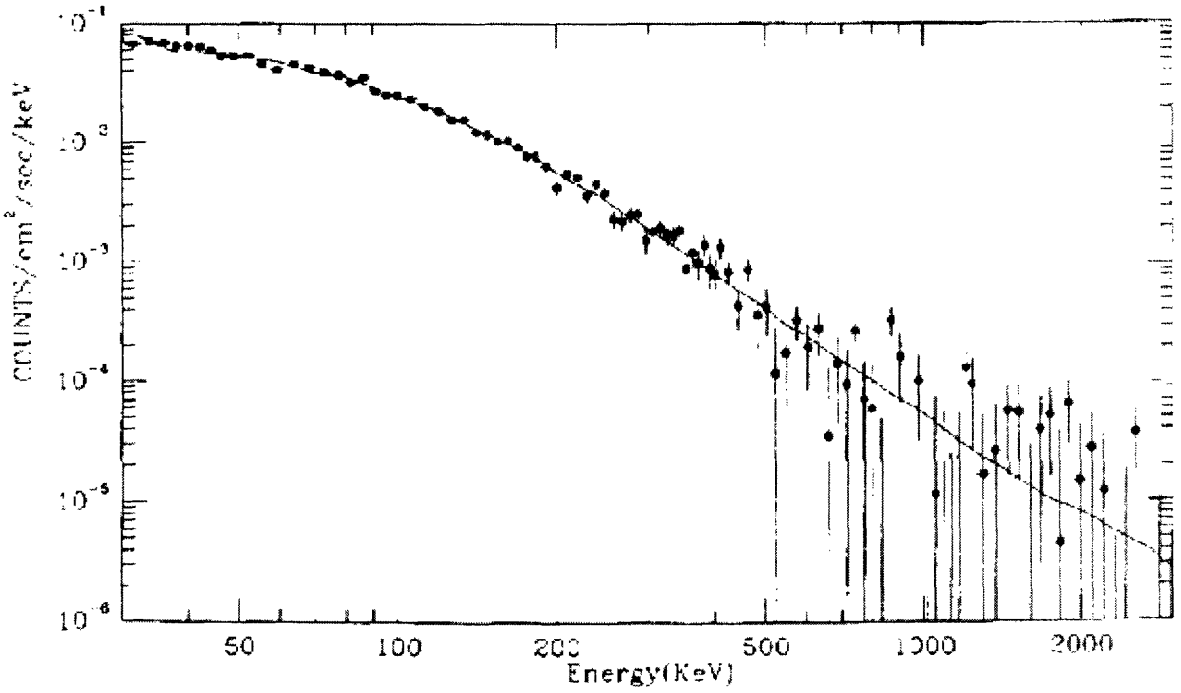

Figure 2-2: *Example of a typical spectral fit for GRB. The shape of a GRB spectrum can be well described, in most cases, by a broken power law joined smoothly at a break energy point (equation 2.10). In this example, the low energy spectral index is* α = -0.968, *the high-energy spectral index is* β = -2.427, *and the break energy is* E_0 = 149.5. *Image courtesy of Band et. al. [27]*

redshifts, z_s. With these source spectra in hand, we then transform them so as to predict what the spectra would look like at an arbitrary redshift, z'. Integration of the redshifted spectra gives the predicted photon flux. Comparing this flux to the detector threshold determines the detectability of the burst at z'. When their ratio is unity, $z' = z_{max}$.

The transformation to arbitrary redshift first involves redshifting the energy, E, of each photon by a factor of $E' = \frac{1+z_s}{1+z'}E$. This effectively shifts the spectra from $N(E)dE$ to $N(E')dE'$. We also need to account for the decrease in number flux of photons due to moving the source further away: the number of detected photons falls off with distance as $\frac{1}{d^2}$, so we multiply the photon count, $N(E')dE'$, by a fac-

tor of $\left(\frac{d_s}{d'}\right)^2$, where d_i is the total line-of-sight comoving distance (equation 2.9) [2]. Integration of $\left(\frac{d_s}{d'}\right)^2 N(E')dE'$ over the appropriate energy interval, unique to each instrument, yields the predicted photon flux for a burst at redshift z'.

A detector's threshold is the minimum count rate that triggers the detector. Because burst count rates are not constant in time and light curves differ for different energy bands, the sensitivity varies with different sets of ΔE and Δt, the energy and time windows in which the burst is incident on the detector. Threshold is dependent on the sensitivity of the instrument, which in turn depends on several parameters, including the total collecting area, detector efficiency, internal background, and average instrument solid angle. The threshold, therefore, is a difficult quantity to model. Band [31] has attempted to model detector thresholds for all GRB detectors to date. Using his results, we model the burst trigger threshold as:

$$S = \frac{F_{Band}}{\sqrt{\Delta t}}. \tag{2.11}$$

where Δt is the burst duration, and F_{Band} represents the detector sensitivity at the peak energy, E_p. This quantity is obtained from Figure 2-3. We lower the threshold by a factor of $\frac{1}{\sqrt{\Delta t}}$ because the longer the detector is registering counts above the background, the more unlikely it is that the detected event is simply a background fluctuation.

Finally, we solve for z_{max} by using a numerical root-extrapolation routine in Matlab, called `fzero`, to drive a burst to the limit of its detectability. We solve for a value of z_{max} such that

$$\frac{\int_{E_1}^{E_2} \left(\frac{d_{obs}}{d_{max}}\right)^2 N(E')dE'}{S} - 1 = 0. \tag{2.12}$$

where d_{max} and E' are functions dependent upon z_{max}.

[2] we adapt terminology from Hogg [25]

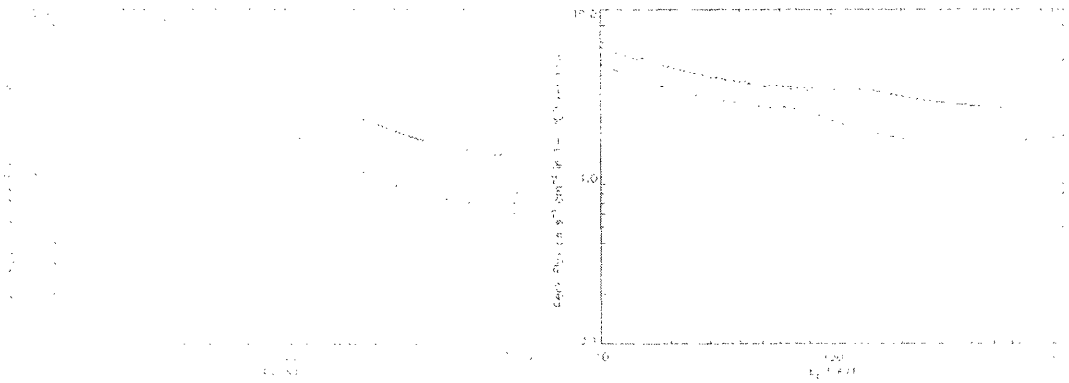

Figure 2-3: *Check this shit out. Graphs of detector thresholds as a function of peak energy, E_p. The graph on the left is for the GRB instrument FREGATE, aboard the HETE-2 mission. The graph on the left is for the GRB monitor aboard the BeppoSAX mission. For each instrument, the solid line represents $\alpha = -1$ and $\beta = -2$, the dashed line $\alpha = -0.5$ and $\beta = -2$, and the dot-dashed line $\alpha = -1$ and $\beta = -3$. α and β represent the high and low energy sprectral parameters, respectively. To obtain F_{Band} for a single burst, we match the known parameters, α and β, to the appropriate line, and read off the threshold at the corresponding peak energy E_p.*

The data for this task were obtained from Frail and Bloom [28]. We note that only some bursts have measured redshifts, and of this set, only some have sufficient spectral-energy parameters published to find z_{max}. We have calculated z_{max} for these bursts and give our results in Table 2.1.

Now with z_{max} in hand, we apply equation 2.7 to all of the bursts in our sample. This gives us the observed volume density, ρ_{obs}. For each instrument, we find that $\eta = \frac{67}{12}$ for HETE-2 and $\eta = \frac{42}{12}$ for BeppoSAX. This yields an observed density of $(\rho_{obs,HETE-2}) = 7.91 \times 10^{-10}$ Mpc^{-3}, and $(\rho_{obs,BeppoSAX}) = 1.18 \times 10^{-10}$ Mpc^{-3}. In the next section, we calculate ΔT, the observation time of detected bursts.

2.1.2 Calculating the total observation time, ΔT

In this section, we calculate the total observation time for the HETE-2 and BeppoSAX missions. Normally, these would be trivial subtractions between the "turn

Burst	Instrument	z_s	z_{max}
970228	BeppoSAX	0.69	1.98
970508	BeppoSAX	0.84	1.28
971214	BeppoSAX	3.42	9.04
980326	BeppoSAX	1.00	1.12
980329	BeppoSAX	2.95	19.89
980613	BeppoSAX	1.10	1.49
990123	BeppoSAX	1.60	26.26
990510	BeppoSAX	1.62	7.62
990705	BeppoSAX	0.84	5.35
990712	BeppoSAX	0.43	1.04
000214	BeppoSAX	0.85	1.83
010222	BeppoSAX	1.48	24.68
010921	HETE-2	0.45	1.38
020124	HETE-2	3.20	1.81
020813	HETE-2	1.25	2.18
021004	HETE-2	2.34	2.66
021211	HETE-2	1.01	1.30
030115	HETE-2	2.20	2.11
030226	HETE-2	1.99	2.34
030324	HETE-2	2.70	2.72
030328	HETE-2	1.52	1.85
030329	HETE-2	0.17	0.83
030429	HETE-2	2.66	2.34
030528	HETE-2	1.00	1.54

Table 2.1: *Measured redshifts, z_s, and maximum detectable redshifts, z_{max}, for GRBs detected by BeppoSAX and HETE-2. Maximum redshifts for bursts detected by other instruments (Integral, and Swift) are unavailable until sufficent data are published from those missions. Data for the results presented in columns 1 - 3 are adapted from Freidmann and Bloom [28]*

on" and "shutdown" dates of the instruments, but literature searches did not yield those dates for our missions. Instead, we will find suitable approximations for ΔT.

HETE-2 had the following history: The first detected burst was GRB 010921, and we last checked for new bursts to incorporate into this thesis on August 28th, 2005, so its effective "turn off" date (since it s still operating) was 2005-08-28. We approximate $\Delta T \approx \Delta\tau + \frac{1}{r}$. $\Delta\tau$ represents the time difference (in years) between the first detected burst and the last time we incorporated new bursts in this analysis ($\Delta\tau = 3.94$ yr), and r represents the an approximation to the average rate of detection for that instrument ($r = \frac{K}{\Delta\tau}$). (Since detectors typically function for some time before the first burst is detected and after the last burst is detected, we assume that the burst occurance intervals follow a Poisson distribution and the average time interval between bursts is thus $\frac{1}{r}$). Thus, we get a total observation time for HETE-2 to be $\Delta T = 4.00$ yr.

BeppoSAX has a simpler history. The instrument BeppoSAX has the following history: The instrument "turn-on" date was 1996-06-03 and the instrument shutdown date was 2004-02-30. Thus, we get a total observation time for BeppoSAX to be $\Delta T = 5.91$ yr.

2.1.3 Calculating the total observed GRB Rate, R_{obs}

Since we have different burst frequencies for each instrument (as expected, since the instrumental sensitivities differ), we will have different GRB rates, R_{obs}. Using equation 2.7, we find that the total rate per unit volume, R_{obs} is the sum of the individual rates:

$$R_{obs} = \left(\frac{\rho_{obs}}{\Delta T}\right)_{HETE-2} + \left(\frac{\rho_{obs}}{\Delta T}\right)_{BeppoSAX} \tag{2.13}$$

Subsituting in values for equation 2.13 gives us a total observed burst rate of $R_{obs} =$

2.18×10^{-10} Mpc^{-3} yr^{-1}.

2.2 Estimating the expected rate of GRBs, R_{exp}

In this section, we calculate the true (or expected) rate (Mpc^{-3} yr^{-1}) of hypernovae, which we postulate to be GRBs. We define a hypernova to be a rapidly rotating, core collapse supernova that ends with the formation of a black hole. We estimate this rate with the following decomposition:

$$R_{exp} = r_p \cdot \beta \cdot f \cdot \rho \tag{2.14}$$

Here, r_p is the Galactic rate of core collapse supernovae (SNe) that end in pulsars; observationally, this is the pulsar birthrate. β is the ratio of SNe in the Galaxy that end in black holes to SNe that end in pulsars. f is the fraction of core collapse SNe in the Galaxy that have cores that are rotating sufficently rapidly to form microquasars when they collapse [16], and ρ is the number density of Milky Way-equivalent galaxies in the universe [3].

In the above decomposition, we have implicitly made several assumptions. We use Milky Way equivalents in our counting procedure, and assume that the comoving number density of Milky Way-equivalent galaxies is constant in time (i.e., no cosmological evolution of either the comoving number density of Milky-Way galaxies or the rate of SN/hypernova production per galaxy). Justification for this assumption is given in Appendix A. By doing this, we also assume that these hypernova candidates are found only in spiral galaxies (See Ch. 1 for a justification of this assumption).

We calculate the, r_p, β, f, and ρ in the following subsections.

[3] By Milky-Way equivalent galaxies, we mean the number of galaxies with Massive Star Formation Rates equal to the current Massive Star Formation Rate in the Galaxy.

2.2.1 Calculating r_p – the Galactic rate of core collapse SNe

Determining the Galactic rate of core collapse SNe is difficult to do directly, and we find counting their end products to be more accessible. Therefore, we use the Galactic pulsar birthrate instead. A pulsar is the product of a moderately massive ($8M_\odot \lesssim M \lesssim 20M_\odot$) core collapse SN, and its population birthrate is well studied.

r_p has upper and lower limits of 1/20 and 1/250 yr^{-1}, respectively, with a best-estimate value around 1/125 yr^{-1} [32, 33, 34, 35]. Later on (Chapter 3), we will assume a probability distribution of values for r_p, based on the upper and lower limits given above.

2.2.2 Calculating β – the Galactic ratio of SNe that produce black holes to SNe that produce pulsars

In our definition for a hypernova, we require that the SN yields a black hole upon death. Black holes are created from SNe with a lower mass limit near 20 $M_\odot$ [36]. In §2.2.1, we obtained a rate for SNe that create pulsars upon death. To convert this SN rate to a black hole birthrate, we multiply our rate by β – the birthrate ratio of black holes to pulsars in the Galaxy. This quantity is found from the Salpeter Initial Mass Function (IMF) [37]. The Salpeter IMF is the integrand of the birthrate density (time^{-1} volume^{-1}) of stars with masses in the range (M, M + dM), and is given by:

$$dN \propto M^{-2.35} dM/dt \tag{2.15}$$

Thus, to determine the birthrate ratio of black holes to pulsars, we simply take the ratio of their predicted birthrates:

$$\beta = \frac{\int_{20-30M_\odot}^{150M_\odot} M^{-2.5} dM}{\int_{8-11M_\odot}^{20-30M_\odot} M^{-2.5} dM} \tag{2.16}$$

To incorporate the uncertainty in the limits of integration, we will assume a uni-

form distribution for their values when we perform the Monte Carlo simulation in Chapter 3.

2.2.3 Calculating f – the fraction of rapidly rotating core collapse SNe

Our hypernova model requires rapid rotation, which begs the question of how a SN progenitor can acquire the necessary rotation speeds to create a hypernova. Even if the progenitor had been rapidly rotating, sustaining large rotational angular velocities is difficult – loss of angular momentum via its stellar wind will leave the star rotating in a state of relatively slow rotation. A better, and more natural, mechanism for rapid rotation in SN progenitor cores is from binary interaction with a companion star [38, 39]. Tidal locking, mass accretion from the companion star, and even the merger of both stars followed by transfer of angular momentum inwards to the stellar core, are viable processes that allow the progenitor to attain and sustain the large angular velocities necessary to form a hypernova [38, 39]. Furthermore, a large fraction of stars are members of binary systems [40, 41, 42], so that a large fraction of massive stars had a binary companion at some point during their lifetime.

In 1992, Podsiadlowski et al. [1] estimated the fraction of core collapse supernovae that originated from binary systems in the Galaxy. Only Type II and Type Ib/c SNe result from core collapse. Of these SN types, we assume that only the accretion and merger processes transfer the neccesary amount of angular momentum to the progenitor star. These processes are labeled as the "SN II (blue)" type in the results of Podsiadlowski et al. given in Table 2.2 below. We use the weighted average values for our parameter f, and use the upper and lower extrema given in the Table as our range of possible values. Thus, f is between 2.4% to 6.4%.

Supernova Type	8–11 $M_\odot$	11–15 $M_\odot$	15–20 $M_\odot$	Weighted Average
A. Assuming One Binary for Every Three Systems				
SN II	88% (87%)	81% (80%)	76% (76%)	83% (83%)
SN II (stripped)	0.5% (0.2%)	1.5% (0.5%)	0.9% (0.3%)	0.9% (0.3%)
SN II (blue)	3.7% (3.4%)	2.0% (1.8%)	3.6% (1.6%)	3.2% (2.4%)
Accretion	1.1% (0.4%)	0.7% (0.2%)	3.2% (1.0%)	1.4% (0.4%)
Merger	2.6% (3.0%)	1.3% (1.6%)	0.4% (0.6%)	1.8% (2.0%)
SN Ib	8.1% (9.4%)	16% (18%)	20% (22%)	13% (15%)
B. Assuming Two Binaries for Every Three Systems				
SN II	73% (71%)	63% (60%)	55% (55%)	66% (64%)
SN II (stripped)	1.2% (0.4%)	3.0% (1.1%)	1.7% (0.6%)	1.9% (0.6%)
SN II (blue)	8.0% (7.6%)	3.9% (3.7%)	6.7% (3.0%)	6.4% (5.1%)
Accretion	2.3% (0.8%)	1.3% (0.4%)	6.0% (2.0%)	2.8% (0.9%)
Merger	5.7% (6.8%)	2.6% (3.3%)	0.7% (1.0%)	3.6% (4.2%)
SN Ib	18% (21%)	31% (35%)	36% (42%)	26% (31%)

Table 2.2: *Shown are the relative frequencies of various core collapse supernova types in systems with massive primaries, based on Monte Carlo simulations of different evolutionary scenarios. The frequencies refer to the percentages of all stars (not systems) that experience a particular type of supernova explosion. We assume that rapid rotation in massive stars is induced from accretion and merger processes. Thus, we use values listed under the "SN II (blue)" category. Adapted from Podsiadlowski et al. [1]*

2.2.4 Calculating ρ – the number density of Milky Way-equivalent galaxies in space

To calculate ρ, we use the galaxy luminosity function, $\Phi(L)$, with spiral galaxy parameters, which gives the number density of spiral galaxies as a function of luminosity. $L\Phi(L)dL$ is the corresponding luminosity density (i.e., the total luminosity per unit volume contributed by galaxies with luminosities between L and $L + dL$). If we also know L_{MW}, the luminosity of the Milky Way, then the number density of Milky-Way-equivalent galaxies is given by

$$\rho = \frac{\int_{L_0}^{\infty} L\Phi(L)dL}{L_{MW}} \tag{2.17}$$

To provide an analytic fit to the data, Schechter [43] proposed the following ap-

proximation:

$$\Phi(L)dL = \phi_* \left(\frac{L}{L_*}\right)^{\alpha} e^{-L/L_*} \frac{dL}{L_*} \tag{2.18}$$

In this expression, ϕ_*, L_*, and α are empirical constants that vary with galaxy morphology. ϕ_* is a normalization factor based on the overall number density of galaxies. L_* is a characteristic (or "modal") galaxy luminosity, and α is the the slope of the luminosity function at L << L_* (i.e., the faint-end slope) – it is a measure of how much mass is locked up in faint galaxies.

Combining equations 2.16 and 2.17, and then simplifying using the incomplete Gamma function, $\Gamma(x)$, we find:

$$\rho = \frac{\phi_* L_* \Gamma(\alpha + 2, \frac{L_0}{L_*})}{L_{MW}} \tag{2.19}$$

where, by definition, $\Gamma(a,x) \equiv \int_x^\infty t^{a-1} e^{-t} dt$. We choose a range of values for L_{MW}, since luminosity estimates depend on the (uncertain) mass of the Galaxy, and adopt it to be $L_{MW} = 2 \times 10^{10} L_{\odot}$. We choose a lower integration limit, L_0, that corresponds to a luminosity of the Small Magellanic Cloud (we have found that evaluation of equation 2.19 is insensitive to the magnitude of L_0). We argue that anything lower would represent a galaxy too small to harbor active star forming regions.

Our final step is to solve for ρ using equation 2.19. From their survey of the nearby optical galaxy sample, Marinoni et al.[44] provide values of α, ϕ_* and M_* (bolometric magnitude) (Table 2.3) under three different velocity field models. To convert from M_* to L_*, we use $M_{solar} = 4.7896$ and the following equation:

$$\frac{L_*}{L_{\odot}} = 10^{-0.4(M_* - M_{solar})} \tag{2.20}$$

THE PARAMETERS OF THE MORPHOLOGICAL TYPE-SPECIFIC LFS.

Model	Sample	Ngal	α	$M_B^* - 5\log h_{75}$	$\phi^*(10^{-4}h_{75}^3 Mpc^{-3})$	χ^2/dof
	E	344	-0.17 ± 0.22	-20.75 ± 0.26	0.46 ± 0.12	0.56
	S0	596	-1.17 ± 0.20	-20.44 ± 0.26	0.81 ± 0.20	0.37
	E-S0	940	-0.97 ± 0.14	-20.69 ± 0.18	1.03 ± 0.24	0.51
Multi-attractor (Mark III)	Sa-Sb	1521	-0.62 ± 0.11	-20.51 ± 0.12	2.20 ± 0.46	0.31
	Sc-Sd	2240	-0.89 ± 0.10	-20.39 ± 0.11	3.12 ± 0.59	0.41
	Sm-Im	619	-2.41 ± 0.28	-21.11 ± 0.72	0.07 ± 0.07	0.68
	S-Im	4380	-1.10 ± 0.07	-20.63 ± 0.09	4.58 ± 0.73	0.63
	E	345	-0.56 ± 0.22	-20.71 ± 0.26	0.45 ± 0.12	0.39
	S0	605	-1.03 ± 0.21	-20.20 ± 0.24	1.03 ± 0.26	0.31
	E-S0	950	-1.03 ± 0.14	-20.67 ± 0.19	1.06 ± 0.25	0.64
Cluster Dipole Model	Sa-Sb	1563	-0.73 ± 0.11	-20.48 ± 0.12	2.21 ± 0.47	0.49
	Sc-Sd	2289	-0.97 ± 0.09	-20.35 ± 0.12	3.17 ± 0.60	1.09
	Sm-Im	597	-2.45 ± 0.32	-21.12 ± 0.73	0.07 ± 0.07	0.64
	S-Im	1449	-1.17 ± 0.08	-20.60 ± 0.09	4.52 ± 0.72	0.89
	E	346	-0.55 ± 0.22	-20.73 ± 0.27	0.45 ± 0.11	0.77
	S0	589	-1.08 ± 0.21	-20.18 ± 0.24	0.79 ± 0.20	0.27
	E-S0	935	-1.12 ± 0.13	-20.72 ± 0.19	0.95 ± 0.23	0.74
Hubble Flow in LG frame	Sa-Sb	1539	-0.78 ± 0.11	-20.57 ± 0.13	2.10 ± 0.44	0.57
	Sc-Sd	2249	-0.93 ± 0.09	-20.33 ± 0.11	3.21 ± 0.61	0.37
	Sm Im	620	-2.27 ± 0.32	-20.75 ± 0.69	0.15 ± 0.15	0.42
	S-Im	4108	-1.17 ± 0.07	-20.60 ± 0.09	4.62 ± 0.70	0.45

Table 2.3: *Measured parameters for the Schechter luminosity function according to morphological type of galaxy. Each of these parameters was deduced using three different velocity models to describe the expansion of the local universe: Multiattractor, Cluster Dipole, and ordinary Hubble Flow. Adapted from Marinoni et al. [44]*

Parameter	Value/Distribution
R_{obs}	2.18×10^{-10} yr^{-1}Mpc^{-3}
L_{MW}	2×10^{10} $L_{\odot}$
M_0	[8,11] $M_{\odot}$
M_1	[20,30] $M_{\odot}$
M_2	150 $M_{\odot}$
r_p	$0.005 \times 10^{[0,1]}$ yr^{-1}
f	[0.024,0.064]
ϕ_*	$[3.80,5.24]\times10^{-3}$Mpc^{-3}
α	[-1.25,-1.09]
M_*	[-20.69, -20.51]

Table 2.4: Monte Carlo parameter distributions

We adopt values specific to S-Im galaxies in Table 2.3, since 1) GRBs have been observed to occur in spiral galaxies only (see Chapter 1), and 2) active star formation is believed to occur only in S-Im galaxies. We use values taken from the Multiattractor model (which is thought to be the most realistic model). Finally, using equations 2.19 and 2.20, and the upper and lower values of α, ϕ_*, and M_* from Table 2.3, we construct probability distributions for use in the Monte Carlo simulation (Chapter 3).

2.2.5 Summary

In §2.1.1 - 2.1.4, we estimated a value, or a range of possible values, for variables needed to calculate R_{exp}. In this section, we estimate those primary quantities in terms of parameters given below.

We adopt the following notation for values given below in Table 2.4: [a,b] represents a uniform distribution of numbers between a and b. Because the pulsar birthrate, r_p, spans over an order of magnitude, we choose a distribution that is uniform in the logarithm.

Chapter 3

Results, Conclusions, & Future Work

3.1 Estimating θ

In this section, we use the results developed in the previous chapter to estimate θ, the jet-opening angle of GRBs. Our expression for calculating θ is given by equation 2.4. Substituting in the appropriate values for R_{exp} (equation 2.14) and R_{obs}, we rewrite θ as:

$$\begin{aligned}
\theta_1 &= 2\cos^{-1}\left(1 - 2\frac{R_{obs}}{r_p \beta f \rho}\right) \\
&= 2\cos^{-1}\left(1 - \frac{2R_{obs}L_{MW}\int_{M_0}^{M_1} M^{-2.5}dM}{r_p f \phi_* L_* \Gamma\left(\alpha+2, \frac{L_0}{L_\odot 10^{-0.4(M_*-M_\odot)}}\right)\int_{M_1}^{M_2} M^{-2.5}dM}\right) \qquad (3.1) \\
\theta_2 &= 2\cos^{-1}\left(1 - \frac{R_{obs}}{r_p \beta f \rho}\right) \\
&= 2\cos^{-1}\left(1 - \frac{R_{obs}L_{MW}\int_{M_0}^{M_1} M^{-2.5}dM}{r_p f \phi_* L_* \Gamma\left(\alpha+2, \frac{L_0}{L_\odot 10^{-0.4(M_*-M_\odot)}}\right)\int_{M_1}^{M_2} M^{-2.5}dM}\right) \qquad (3.2)
\end{aligned}$$

Many of these variables have ranges of possible values, given in Table 2.4. To

incorporate their range, we perform a Monte Carlo simulation to estimate θ in the following way: Using these ranges of possible values, we assume that each variable has a specific probability distribution of values within its estimated range. We then choose at random a possible value for each of the variables and use equation 3.1 to calculate θ. We repeat this process 10,000 times and plot the resulting frequency distribution of θ as a histogram (Figure 3-1).

Since the number of jets emitted by a γ-ray burst source is uncertain, we perform a Monte Carlo simulation and estimate θ for both the single and double jet models. Recall that in the limit of small θ, $\theta_1 \simeq \sqrt{2}\theta_2$. Our results from this are given below in Figure 3.1. For each distribution, there exists a median value of θ and a most frequent value of θ that represents the most probable value. For the single-jet burst model, we find that the most probable value is 8^{+6}_{-3} deg (FWHM), the median value is 10.3 deg, and the standard deviation is 4.4 deg. For the double-jet model, we find that the most probable and median values are $5.5^{+3}_{-1.5}$ deg, and 7.3 deg, respectively, and a standard deviation of 3.1 deg.

3.2 Discussion

Recently, Frail et al. [3] estimated opening angles, θ_j, for a set of GRBs with known redshifts, concluding that in most cases $3^\circ < \theta_j < 25^\circ$, with a significant concentration at roughly 4°. Their estimate of θ_j was based on measuring physical properties of the GRB jet, and contain no information about the existence of an opposing (double) jet. Our values for θ_j are consistent with their measured result. It is thus very plausible, under the assumptions that we have made in this thesis, that the hypernova population and the GRB population are one and the same. More importantly, this result demonstrates that the hypothesis that the origin of hyernova in massive interacting binary systems is consistent with the observational results of Frail et al. [3].

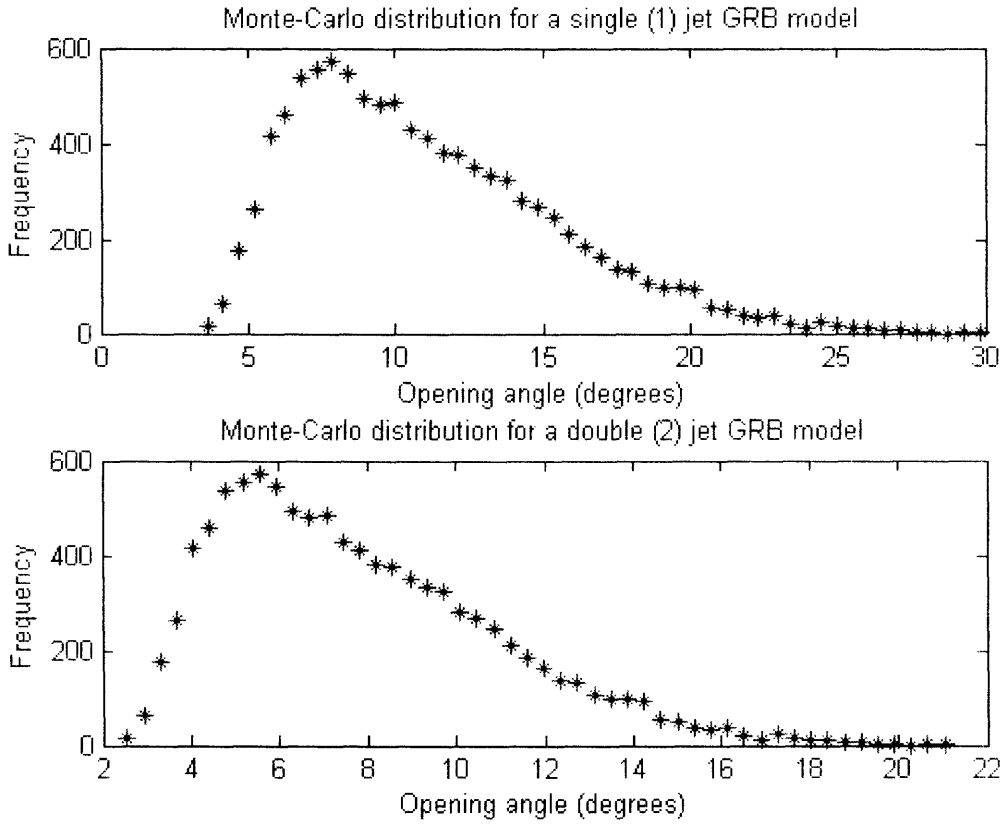

Figure 3-1: The Monte Carlo distribution of possible values of θ for single and double jet models.

Our results from the Kolmogorov-Smirnov test (Appendix A) have implications for the constancy over cosmological timescales of the rate of occurence of hypernova progenitors. Our results show that GRBs, and, by implication, hypernova progenitors, have no significant cosmological evolution (i.e. the comoving number density is constant over the time that we can access with the current sample of GRBs to $z \simeq 3$). If our hypothesis that hypernovae are the progenitors of GRBs is correct, then these results also imply that the rate of massive star formation in S-Im galaxies has not changed over time. Of course, individual spiral galaxies may still evolve, but the overall birthrate of massive stars in such galaxies does not appear to have changed significantly.

3.2.1 Was Supernova 1987A a Hypernova?

SN 1987A was the closest naked-eye supernova in over 300 years, occuring in the Large Magellanic Cloud. The energies and temporal spread of neutrinos detected from the explosion provided strong confirmation of the core collapse theory for massive SNe. However, in many ways SN 1987A did not comply with theoretical expectations for a core collapse SN. In particular, its progenitor, Sk $-69^{\circ}202$, was a blue supergiant, rather than the red supergiant that had been expected.

In 1992, Podsi et al [6] argued that the progenitor of SN 1987A had undergone accretion from, or merger with, a binary companion. This raises the possibility that SN 1987A could have been a (possibly failed) hypernova[1].

The empirical evidence suggests a strong connection among supernovae, hypernovae, and GRBs. Our candidates for hypernova progenitors are massive stars that aquired rapid core rotation through interaction with a past or present binary companion, and Sk $-69^{\circ}202$ seems to have been a member of this class. We summarize below the evidence in support of this assertion.

1) **Core collapse** is by definition a prerequisite for the evolution of a hypernova [16]. From the nature of its neutrino emission [45, 46], we know that the progenitor of SN 1987A experienced core collapse.

2) **Prior Binary Membership.** There are two main reasons to believe that Sk $-69^{\circ}202$ had a binary companion. The blue color of Sk $-69^{\circ}202$, the rapid rise time of the optical SN outburst, and the rapid decline of the SN lightcurve, all serve as direct observational evidence to support this belief [6]. Additionally, subsequent to the supernova explosion, the surrounding ejecta took an axially symmetric form

[1] We define a "failed" hypernova as a hypernova event that generates only weak jets (and, perhaps, a correspondingly weak GRB event) or no jets at all. This is possible if some or all of the hypernova jet energy is absorbed by the stellar envelope, either because the hypernova event is relatively weak or because the stellar envelope is relatively thick.

(Figure 3.2.1), which is to be expected if Sk $-69^{\circ}202$ was the product of a merger in a massive binary system [1].

3) **Rapid Rotation** of the progenitor core is a prerequisite for a hypernova [16]. Sk $-69^{\circ}202$ appears to have been the product of a binary merger [1]. Via transfer of angular momentum, such mergers result in a rapidly rotating blue supergiant. [1, 39, 6, 38].

4)) **Signs of a relativistic jet.** In 1987, a "mystery spot" was found in images of SN 1987A [47]. A subsequent re-analysis of the data [48] found a second such spot on the opposite side of SN 1987A. The line connecting these two spots is nearly parallel to the symmetry axis of the pre-supernova ejecta, which is presumably the axis of rotation of the progenitor star. This suggests that the spots delineate a jet receding obliquely from us (the observer). Furthermore, the spots were also found on an image taken at a later date, enabling the speeds of the moving spots to be calculated [2]. These speeds were found to be $1.2c$ and $0.6c$. Such transluminal velocities are suggesetive of jets similar to those believed to occur in hypernovae. If one of these jets had been aimed along our line of sight, we might have observed a GRB coincident with SN 1987A.

In this thesis, we have found that if GRBs are produced by massive interacting binaries, then the GRB jet opening angle is consistent with that found from independent arguments. Thus, our results lend additional weight to the hypothesis that SN 1987A was a prototypical hypernova event that generated relativisitic jets, possibly producing GRBs for observers within the beams of the jets.

3.2.2 Future Work

With so many variables in play, the direction of future efforts should be toward sensitivity analysis. Attention should first be given to the variables with the largest effect

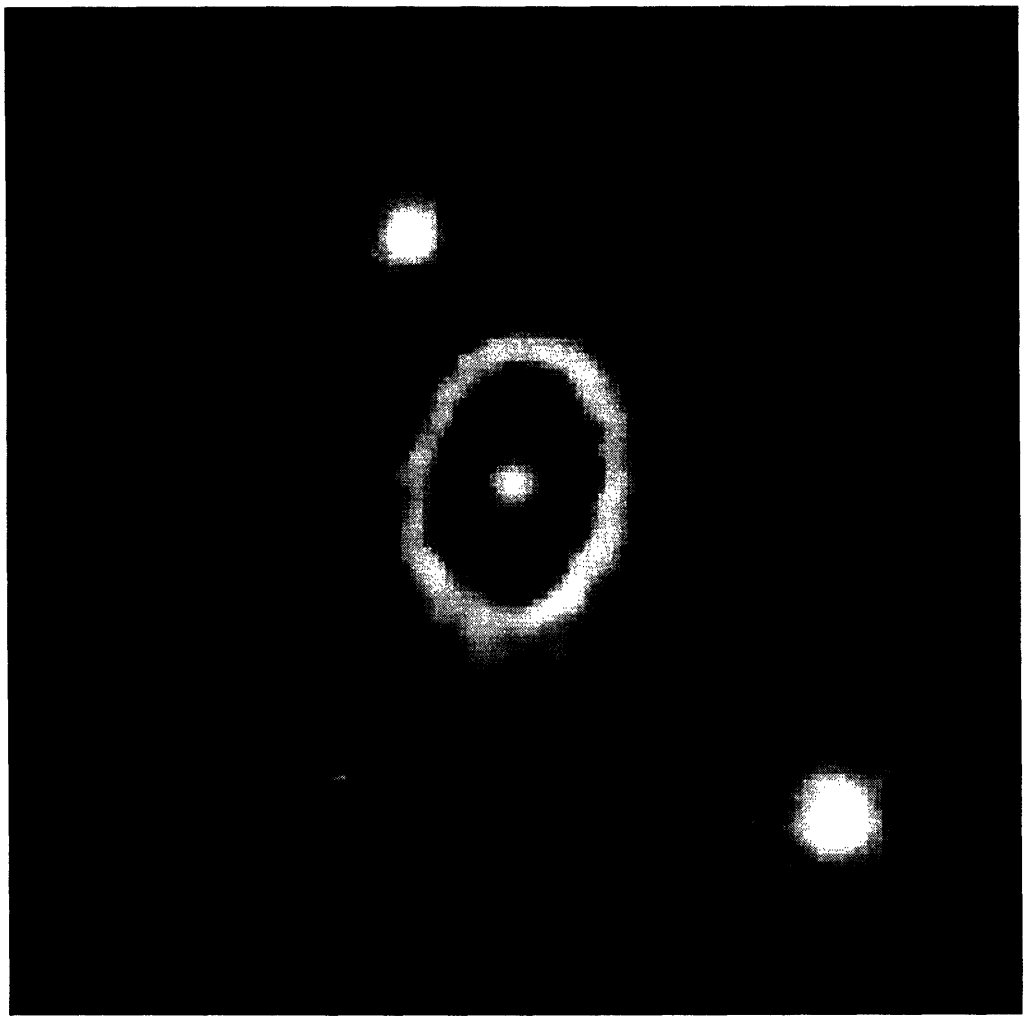

Figure 3-2: *The aspherical, axisymmetric distribution of ejecta around SN 1987A implies a rapidly rotating progenitor star. Photo taken by the Hubble Space Telescope, courtesy of the Space Telescope Science Institute (STScI)*

on the final answer. Assumptions and estimates surrounding those variables require the most scrutiny.

There are a few particular assumptions and approximations that need to be refined. These are listed below:

When calculating ρ (§2.3), we assumed that its value is independent of redshift. If, however, galactic number density varies with redshift (as seems likely), then equation

2.19 would require revision. (On the other hand, our results of for the $\frac{V}{V_{max}}$ suggest that the overall GRB rate has been constant in time.)

Our z_{max} values are highly sensitive to the photon flux threshold of each GRB instrument (equation 2.11). Figure 2-3 was given by Band et al. [31] and was derived by integrating over a common energy band. However, each instrument does not cover such a wide energy window. For example, Band et al.'s [31] functions yield non-zero detection rates for bursts with peak energies clearly outside the energy band of the instrument. Their technique should be repeated with greater care, so that each instrument has its own specific energy band taken into account. This should reduce the systematic errors in z_{max}, which we suspect may be substantial.

We can improve our counting statistics by taking Swift data into account. At the time of this writing, data from the Swift mission is not yet publicly available. As Swift has already measured redshifts for more GRBs than any other instrument, data from this mission will significantly improve our z_{max} statistics. For example, in just six months of operation, Swift has data for fifteen bursts with measured redshifts using these data will nearly double our exisiting sample size. Inclusion of Swift data makes the missing spectral parameters of HETE-2 and BeppoSAX almost irrelevant.

We need to incorporate the newest estimates for the range of values for the mass cutoffs (M_1 and M_2) for black hole formation in supernova events (equation 2.16).

Finally, when calculating ρ, we applied a single luminosity function and birthrate for S-Im galaxies. A good refinement would be to implement the appropriate luminosity function and birthrate for each galaxy type separately.

Appendix A

Distribution of $\frac{V}{V_{max}}$

How are GRBs and their progenitors distributed thoughout space? Is their spatial density uniform, or do evolutionary effects come into play? In this section, we test the hypothesis that GRBs and their progenitor systems are uniformly distributed thoughout space (i.e., homogeneous). To do this, we make use of the $\frac{V}{V_{max}}$ statistic and utilize a statistical method (the Kolmogorov-Smirnov test) to determine the likelihood of this assumption.

The $\frac{V}{V_{max}}$ test was first introduced to astrophysics by Schmidt in 1968 [49] to measure the spatial distribution of distant quasars. It is a method that gives a quantitative measure of the uniformity of the radial distribution of the parent population of a set of observed objects. Empirically, it is the ratio of the comoving volume V enclosed at a cosmological redshift z, to a maxiumum volume V_{max} enclosed at a redshift z_{max} that represents the maximum distance at which a given object would be seen.

The distribution of $\frac{V}{V_{max}}$ for a set of observed objects can tell us about their uniformity in space. For example, if a sample of objects is drawn from a parent population with a uniform distribution, then the $\frac{V}{V_{max}}$ values for that sample will be uniformly distributed between 0 and 1, which gives a mean $\frac{V}{V_{max}}$ of 0.5. A sample with a small (< 0.5) mean value of $\frac{V}{V_{max}}$ means that most of these objects prefer a nearer part

of their accessible volume. This implies that the objects were either more rare or intrinsically fainter in the past. Since GRBs are a stellar phenomenon, we do not not anticipate that their instrinsic luminosities would change, and assume that any deviation of the mean from 0.5 represents a change in density evolution instead. Similarly, a sample with a larger (> 0.5) mean would imply that the objects were more commonplace in the past. In either case, a non-uniform parent population distribution would be indicated, so that evolutionary effects may need to be taken into account.

In this thesis, we consider the $\frac{V}{V_{max}}$ values for the set of GRBs with known redshifts (studied in Chapter 2). If these GRBs were derived from systems with a homogenous spatial distribution, then our $\frac{V}{V_{max}}$ values for GRBs would be uniformly distributed between 0 and 1 and would have an average value of 0.5. We test this hypothesis by using the Kolmogorov-Smirnov one-sample test [50, 51] (hereon the K-S test).

The K-S test is a statistical test that gives a measure of goodness of fit. It allows one to determine whether a sample of objects is consistent with a given theoretical parent population. This is done by comparing the observed cumulative frequency distribution (cdf) $F_0(x)$ with a predicted theoretical cdf $F(x)$. Here, $F_0(x)$ and $F(x)$ are defined to be the fractional number of actual and expected observations, respectively, with values equal to or less than x. For our current problem, $x = \frac{V}{V_{max}}$ and $F(x) = x$ (for $0 \leq x \leq 1$). By measuring the maximum deviation between the two distributions, one can determine the probability for such a difference to occur if the observations were really a random sample drawn from the parent population. We use the K-S test on our sample of GRBs to test the hypothesis that these observed bursts are derived from a parent population that is uniformly distributed throughout comoving space.

$F_0(x)$, is created from the data presented in Table A.1. Both of $F_0(x)$ and $F(x)$ are shown in Figure A-1. From the figure, the maximum absolute deviation between the two distributions is measured to be $D_n = 0.1410$.

The next step in the K-S test is to determine of obtaining the value of D_n equal to or greater than the actual value if the observed sample was, indeed, randomly sampled from the parent population. The essence of the K-S test lies in the proof that [50]:

$$\alpha(t) = 1 - 2\sum_{i=0}^{\infty}(-1)^{i-1}e^{-2i^2t^2} \tag{A.1}$$

where $t = \sqrt{n}D_n$, n is the total number of observations in the sample, and α is the significance level for a given value of t. The significance level can be interpreted as the probability of incorrectly rejecting the null hypothesis. In other words, the null hypothesis is likely to be accepted for "large" values of α. Here, the null hypothesis is the proposition that our set of observed GRBs is uniformly distributed in comoving space.

Our set of observed GRBs has $n = 24$ samples, so that $\sqrt{n}D_n = 0.6908$. Evaluation of equation A.1 then gives $\alpha(\sqrt{n}D_n) = 0.7266$. Hence, we accept the null hypothesis that GRBs are derived from a population with uniform comoving spatial density. This result means that if a sample of GRBs were drawn from a distribution that has uniform spatial density, then a value of $\sqrt{n}D_n$ equal to or larger than the one we found would be obtained 73% of the time.

Table A.1: Observed cumulative frequency distribution data

$F_0(\mathrm{x})$	$\mathrm{x} = \frac{V}{V_{max}}$
$\frac{1}{24}$	0.0237
$\frac{2}{24}$	0.0832
$\frac{3}{24}$	0.0937
$\frac{4}{24}$	0.1037
$\frac{5}{24}$	0.1127
$\frac{6}{24}$	0.1656
$\frac{7}{24}$	0.1676
$\frac{8}{24}$	0.1945
$\frac{9}{24}$	0.2573
$\frac{10}{24}$	0.2757
$\frac{11}{24}$	0.3732
$\frac{12}{24}$	0.4494
$\frac{13}{24}$	0.4673
$\frac{14}{24}$	0.4845
$\frac{15}{24}$	0.6027
$\frac{16}{24}$	0.6449
$\frac{17}{24}$	0.6696
$\frac{18}{24}$	0.7507
$\frac{19}{24}$	0.8038
$\frac{20}{24}$	0.8229
$\frac{21}{24}$	0.8533
$\frac{22}{24}$	0.9927
$\frac{23}{24}$	1.0000
$\frac{24}{24}$	1.0000

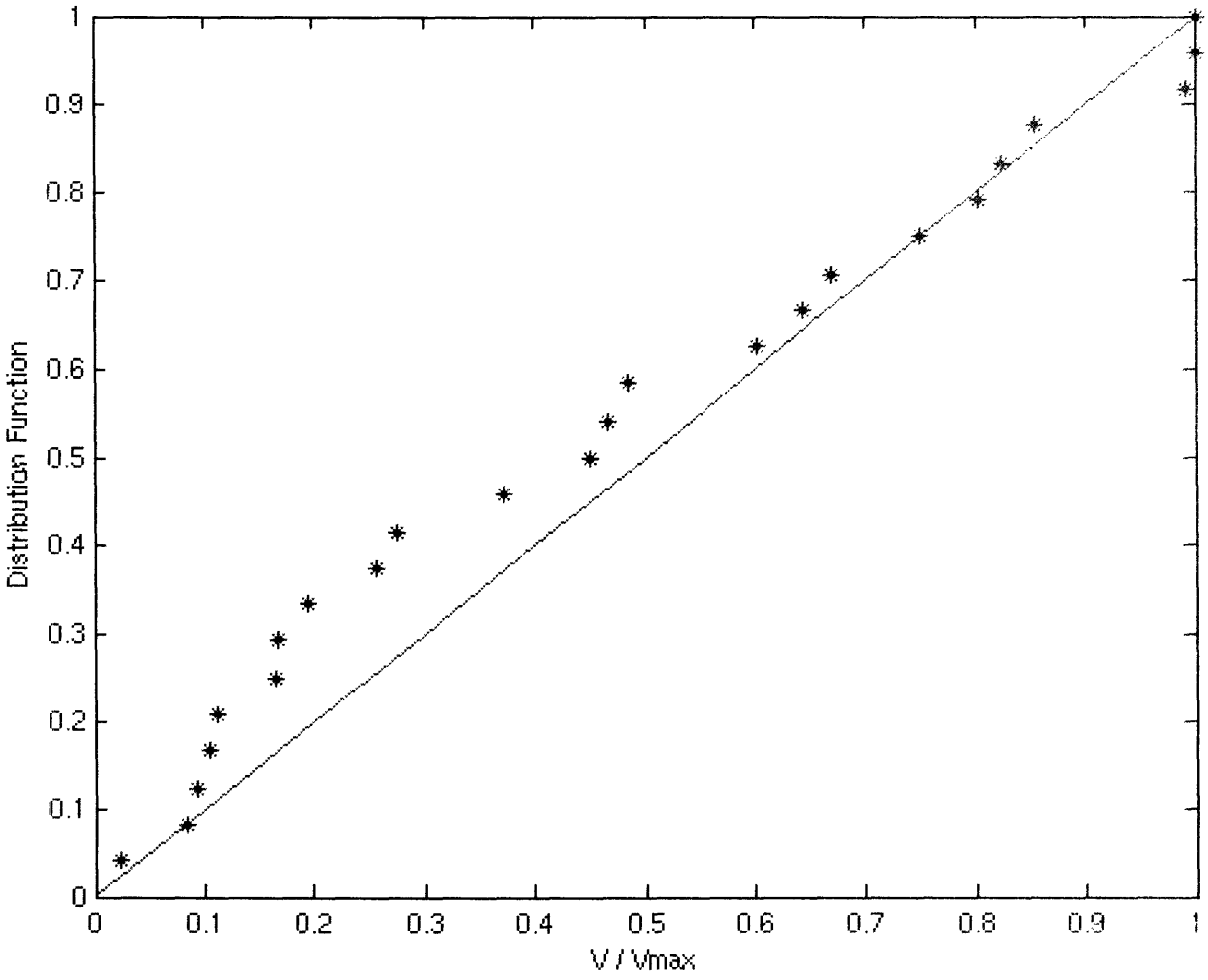

Figure A-1: *Comparison of cumulative distribution functions $F_0(x)$ and $F(x)$. The observed cumulative distribution function (cdf) $F_0(x)$, denoted by asterisk's, represents the cdf for the set of GRBs with known redshifts. The theoretical cdf for a parent population $F(x)$, denoted by the solid line, represents a population of GRBs with uniform comoving spatial density.*

Bibliography

[1] Philipp Podsiadlowski, Paul Joss, and J. J. L. Hsu. Presupernova evolution in massive interacting binaries. *Astrophysical Journal*, 391:246, May 1992.

[2] Renyue Cen. A possible lateral gamma-ray burst jet from Supernova 1987A. *Astrophysical Journal*, 524:L51, 1999.

[3] D.A. et al. Frail. Beaming in gamma-ray bursts: Evidence for a standard energy reservoir. *Astrophysical Journal*, 562:L55, 2001.

[4] R. Perna, R. Sari, and D. Frail. Jets in GRBs: Tests and predictions for the structured jet model. *astro-ph/0305145*, 2003.

[5] Bing Zhang and Peter Meszaros. Gamma-ray burst beaming: a universal configuration with a standard energy reservoir? *Astrophysical Journal*, 571:876 879, 2002.

[6] Phillip Podsiadlowski. The progenitor of SN 1987 A. *Publications of the Astronomical Society of the Pacific*, 104:717 729, September 1992.

[7] R. W. Klebesadel, I. B. Strong, and R. A. Olson. Observations of gamma-ray bursts of cosmic origin. *Astrophysical Journal*, 182:L85, 1973.

[8] E. Mazets et al. Catalog of cosmic gamma-ray bursts from the KONUS experiment data. Part IV. *Astrophysical and Space Sciences*, 80:119, 1981.

[9] K. et al. Hurley. The solar X-ray/cosmic gamma-ray burst experiment aboard ULYSSES. *Astronomy & Astrophysics*, 92:401, 1992.

[10] Bohdan Paczynski. How far away are gamma-ray bursters? *astro-ph/9505096*, 1995.

[11] C. Kim, V. Kalogera, D. Lorimer, M. Ihm, and K. Belczynski. The galactic double-neutron-star merger rate: Most current estimates. *ASP Conference Series*, 328, 2005.

[12] Shinichiro Ando. Short gamma-ray bursts as a possible probe of binary neutron star mergers. *Journal of Cosmology and Astroparticle Physics*, JCAP06(2004)007, 2004.

[13] R. Voss and T. M. Tauris. Galactic distribution of merging neutron stars and black holes – prospects for short γ-ray burst progenitors and LIGO/VIRGO. *Monthly Notices of the Royal Astronomical Society*, 342:1169, 2003.

[14] F. J. Castander and D. Q. Lamb. A photometric investigation of the GRB970228 afterglow and the associated nebulosity. *astro-ph/9807195*, 1998.

[15] D. Q. Lamb, Francisco J. Castander, and Daniel E. Reichart. GRB 970228 and GRB 980329 and the nature of their host galaxies. *astro-ph/9909027*, 1999.

[16] Bohdan Paczynski. Are gamma-ray bursts in star forming regions? *Astrophysical Journal*, 494:L45, 1998.

[17] K. C. et al. Sahu. The optical counterpart to gamma-ray burst GRB970228 observed using the Hubble Space Telescope. *Nature*, 387:476, 1997.

[18] A. S. et al. Fruchter. The fading optical counterpart of GRB 970228, 6 months and 1 year later. *Astrophysical Journal*, 516:683, 1999.

[19] K.R. et al. Kulkarni. The gamma-ray burst of 980425 and its association with the extraordinary radio emission from a most unusual supernova. *Nature*, 395:663, 1998.

[20] J. S. Bloom, S. R. Kulkarni, and S. G. Djorgovski. The redshift determination of GRB 990506 and GRB 000418 with the Echellete Spectrograph Imager on Keck. *Astronomical Journal*, 123:1111, 2002.

[21] S. E. Woosley, N. Langer, and T. A. Weaver. The evolution of massive stars including mass loss - presupernova models and explosion. *Astrophysical Journal*, 411:823, 1993.

[22] R. D. Blandford and R. L. Znajek. Electromagnetic extraction of energy from kerr black holes. *Monthly Notices of the Royal Astronomical Society*, 179:433 456, 1977.

[23] M. H. P. M. van Putten. Gamma-ray bursts: Ligo/virgo sources of gravitational radiation. *Physics Reports*, 345:1–59, 2001.

[24] K.Z. et al. Stanek. Spectroscopic discovery of the supernova 2003dh associated with GRB 030329. *Astrophysical Journal*, 591:L17, 2003.

[25] David Hogg. Distance measures in cosmology. *astro-ph/9905116*, 1999.

[26] C. L. Bennett et. al. First year Wilkinson Microwave Anisotropy Probe (WMAP) observations: Preliminary maps and basic results. *The Astrophysical Journal Supplement Series*, 148:1–27, September 2003.

[27] David Band et. al. Batse observations of gamma-ray burst spectra. i - spectral diversity. *The Astrophysical Journal*, 413:281–292, August 1993.

[28] A. S. Friedman and J. S. Bloom. Toward a more standardized candle using gamma-ray burst energetics and spectra. *The Astrophysical Journal*, 627:1–25, July 2005.

[29] T. Sakamoto et. al. Global characteristics of x-ray flashes and x-ray-rich grbs observed by hete-2. *astro-ph/0409128*, 2004.

[30] L. Amati et al. Intrinsic spectra and energetics of bepposax gamma-ray bursts with known redshifts. *Astronomy and Astrophysics*, 390:81–89, July 2002.

[31] David L. Band. Comparison of the gamma-ray burst sensitivity of different detectors. *The Astrophysical Journal*, 588:945–951, May 2003.

[32] W. Wang, Z. J. Jiang, and K. S. Cheng. Contribution to diffuse gamma-rays in the Galactic Centre region from unresolved millisecond pulsars. *Monthly Notices of the Royal Astronomical Society*, 358:263, March 2005.

[33] Philip Kaaret. The unidentified galactic EGRET sources. *Advances in Space Research*, 21:237–240, 1998.

[34] W. Bednarek and M. Bartosik. Cosmic rays from galactic pulsars. *Astronomy and Astrophysics*, 423:405–413, May 2004.

[35] S. N. Nazin and K. A. Postnov. High neutron star birth velocities and gravitational radiation during supernova explosions. *Astronomy and Astrophysics*, 317:L79–L81, 1997.

[36] Nils Andersson and Kostas D. Kokkotas. Gravitational wave astronomy: the high frequency window. *The Physics of the Early Universe*, 653:255, 2005.

[37] Edwin E. Salpeter. The luminosity function and stellar evolution. *The Astrophysical Journal*, 121:161–167, January 1955.

[38] P. C. Joss and J. A. Becker. Formation and evolution of hypernova progenitors in massive binary systems. In *From Twilight to Highlight: They Physics of Supernovae. Proceedings of the ESO/MPA/MPE Workshop*, 2002.

[39] J.A. Becker. Formation and evolution of hypernova progenitors in massive binary systems. PhD. thesis, Massachusetts Institute of Technology, June 2004.

[40] H. A. Abt and S. G. Levy. Multiplicity among solar-type stars. *Astrophysical Journal Supplement Series*, 30:273–306, 1976.

[41] Z. T. Kraicheva, E. I. Popova, A.V. Tutukov, and L. R. Yungelson. Some properties of spectroscopic binary stars. *Soviet Astronomy*, 22:670–677, 1978.

[42] A. Duquennoy and M. Mayor. Multiplicity among solar-type stars in the solar neighbourhood. ii - distribution of the orbital elements in an unbiased sample. *Astronomy and Astrophysics*, 248:485–524, 1991.

[43] P. Schechter. An analytic expression for the luminosity function for galaxies. *Astrophysical Journal*, 203:297, 1976.

[44] Christian Marinoni, Pierluigi Monaco, Giuliano Giuricin, and Barbara Costantini. The nearby optical galaxy sample: The local galaxy luminosity function. *Astrophysical Journal*, 521:50, 1999.

[45] H.-Thomas Janka. Neutrinos from SN 1987A: Can they tell even more? Talk presented at the Workshop on 'Astro-Particle Physics,' Ringberg Castle, Tegernsee, March 6-10 1995.

[46] Michael Zeilik and Steven A. Gregory. *Introductory Astronomy and Astrophysics*. Brooks/Cole, fourth edition, 1998.

[47] P. Nisenson et al. Detection of a very bright source close to the LMC' supernova SN 1987A. *Astrophysical Journal*, 320:L15, 1987.

[48] Peter Nisenson and Costas Papaliolios. A second bright source detected near SN 1987A. *astro-ph/9904109*. 1999.

[49] Maarten Schmidt. Space distribution and luminosity functions of quasi-stellar radio sources. *Astrophysical Journal*. 151:393, February 1968.

[50] Morris H. Degroot. *Probability and Statistics*. Addison-Wesley, second edition. 1986.

[51] Sidney Siegel. *Nonparametric statistics for the behavioral sciences*. McGraw-Hill. first edition, 1956.